AGU PUBLICATIONS

Water Resources Research

RESEARCH ARTICLE

10.1002/2015WR018499

Key Points:

- The emergence of distinct instabilities
- Measured pressure signatures that differ significantly from those computed based on Laplacian capillarity and constriction geometry
- Transient surfactant conditions as the interface traverses the pore throat

Correspondence to:
J. Jang,
junbong.jang8@gmail.com

Citation:
Jang, J., Z. Sun, and J. C. Santamarina (2016), Capillary pressure across a pore throat in the presence of surfactants, *Water Resour. Res.*, *52*, 9586–9599, doi:10.1002/2015WR018499.

Received 12 DEC 2015
Accepted 17 NOV 2016
Accepted article online 22 NOV 2016
Published online 25 DEC 2016

Capillary pressure across a pore throat in the presence of surfactants

Junbong Jang[1], Zhonghao Sun[1], and J. Carlos Santamarina[1]

[1]Earth Science and Engineering, KAUST, Thuwal, Saudi Arabia

Abstract Capillarity controls the distribution and transport of multiphase and immiscible fluids in soils and fractured rocks; therefore, capillarity affects the migration of nonaqueous contaminants and remediation strategies for both LNAPLs and DNAPLs, constrains gas and oil recovery, and regulates CO_2 injection and geological storage. Surfactants alter interfacial tension and modify the invasion of pores by immiscible fluids. Experiments are conducted to explore the propagation of fluid interfaces along cylindrical capillary tubes and across pore constrictions in the presence of surfactants. Measured pressure signatures reflect the interaction between surface tension, contact angle, and the pore geometry. Various instabilities occur as the interface traverses the pore constriction, consequently, measured pressure signatures differ from theoretical trends predicted from geometry, lower capillary pressures are generated in advancing wetting fronts, and jumps are prone to under-sampling. Contact angle and instabilities are responsible for pronounced differences between pressure signatures recorded during advancing and receding tests. Pressure signatures gathered with surfactant solutions suggest changes in interfacial tension at the constriction; the transient surface tension is significantly lower than the value measured in quasi-static conditions. Interface stiffening is observed during receding fronts for solutions near the critical micelle concentration. Wetting liquids tend to form plugs at pore constrictions after the invasion of a nonwetting fluid; plugs split the nonwetting fluid into isolated globules and add resistance against fluid flow.

1. Introduction

A gas-liquid or a liquid-liquid interface invades a pore when the pressure difference between the two fluids overcomes the capillary pressure. Capillarity controls the migration and distribution of nonaqueous contaminants in soils and fractured rocks, and subsequent remediation strategies for both LNAPLs and DNAPLs [*Essaid et al.*, 1993; *Glass et al.*, 2000; *Mulligan et al.*, 2001; *Saenton et al.*, 2002; *Reddy and Saichek*, 2003; *Li et al.*, 2005; *Daniel et al.*, 2015; *Essaid et al.*, 2015], gas migration, air invasion and desiccation of near-surface soils [*Gens*, 2010; *Likos and Lu*, 2004; *Lu and Likos*, 2004; *Shin and Santamarina*, 2010], gas and oil recovery [*Iglauer et al.*, 2010; *Hirasaki et al.*, 2011; *Johannessen and Spildo*, 2013], and CO_2 injection and geological storage [*Pruess and Garcia*, 2002; *Nordbotten et al.*, 2005; *Kim and Santamarina*, 2014].

The capillary pressure P_c [Pa] in a cylindrical pore of radius r [m] depends on the contact angle θ and the interfacial tension T_{lg} [N/m] between the two fluids as predicted by Young-Laplace's equation $P_c = 2T_{lg}\cdot\cos\theta\cdot r^{-1}$, where $\cos\theta = (T_{ls} - T_{gs})/T_{gl}$ relates the interfacial tensions that arise between the two fluids "g and l" and the solid "s." Surface tension and contact angle are affected by interfacial conditions, roughness, wettability, gas pressure, impurities, and surfactants [*De Gennes*, 1985; *Sharma and Ross*, 1991; *Kwok and Neumann*, 2000; *Miwa et al.*, 2000; *Siebold et al.*, 2000; *Espinoza and Santamarina*, 2010]. Furthermore, both surface tension and contact angle vary as the system changes from static to dynamic conditions (static interfacial tension [*Young*, 1804; *Good*, 1966; *Vargaftik et al.*, 1983], dynamic interfacial tension [*Caskey and Barlage*, 1971; *Bechtel et al.*, 2002], and static versus dynamic wettability [*Wenzel*, 1936; *Cassie and Baxter*, 1944; *Rose and Heins*, 1962; *Hoffman*, 1975; *De Gennes*, 1985]). In noncylindrical tubes, capillary pressure and fluid invasion reflect the irregular cross section of pores as well as their converging-diverging longitudinal geometry [*Ransohoff and Radke*, 1988a; *Mason and Morrow*, 1994; *Dong and Chatzis*, 1995; *Weislogel and Lichter*, 1998; *Bico and Quere*, 2002; *Song and Kovscek*, 2015; *Zhao et al.*, 2016].

Capillary forces, viscous forces, and inertial forces combine to determine capillary rise [*Thomson*, 1886; *Washburn*, 1921; *Siebold et al.*, 2000; *Xue et al.*, 2006], displacement patterns in multiphase flow in porous

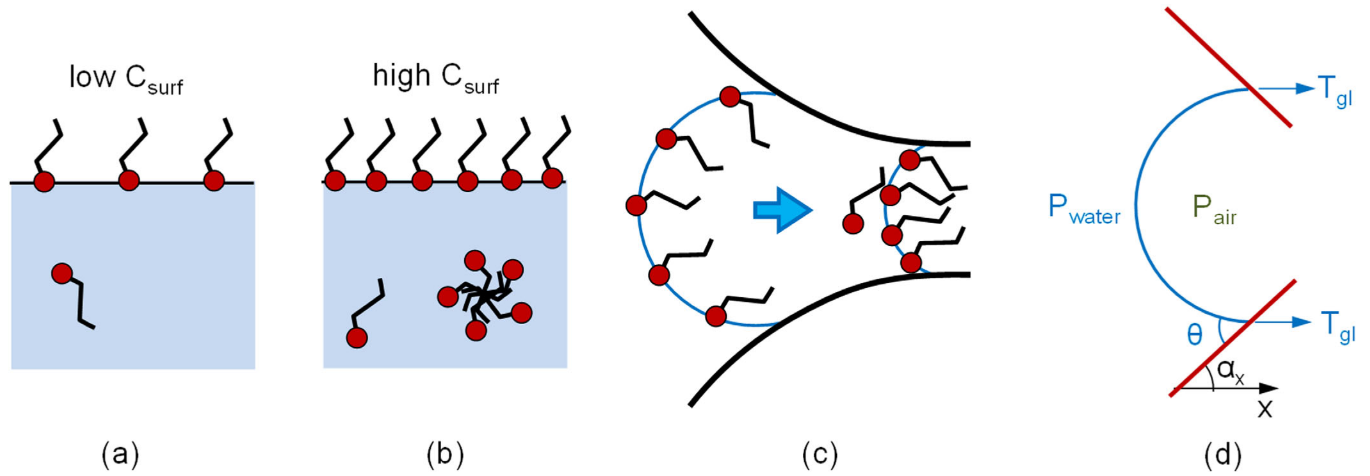

Figure 1. Surfactant interactions at the molecular scale. (a) Preferential adsorption at interfaces. (b) Micelle formation in the bulk solution. (c) Hypothesized transient change in surfactant surface density as the interface traverses the pore constriction. (d) Interface between two fluids at a noncylindrical pore geometry.

media [*Chatzis and Dullien*, 1983; *Stokes et al.*, 1986; *Lenormand et al.*, 1988; *Sandnes et al.*, 2011; *Holtzman et al.*, 2012; *Trojer et al.*, 2015], and various pore-scale phenomena and instabilities such as:

1. *Haines jump*. Sudden changes in pressure and associated abrupt changes in fluid distribution [*Haines*, 1930; *Morrow*, 1970; *Gauglitz and Radke*, 1989; *Maloy et al.*, 1992; *Furuberg et al.*, 1996; *Berg et al.*, 2013].
2. *Snap-off*. An advancing nonwetting fluid becomes discontinuous going through the pore throat as wetting fluid flowing along corners and crevices reaches the pore throat and pinches the nonwetting fluid [*Roof*, 1970; *Lenormand et al.*, 1983; *Ransohoff et al.*, 1987; *Rossen*, 2003; *Valvatne and Blunt*, 2004; *Kovscek et al.*, 2007].
3. Lamella and foam generation and transport [*Falls et al.*, 1988; *Ransohoff and Radke*, 1988b; *Kovscek and Radke*, 1994; *Rossen*, 2003].

Surfactants hinder the development of capillary pressure and facilitate mixed-phase fluid flow in porous media. Surfactants tend to migrate toward gas-liquid "gl" interfaces because of their amphipathic structure with hydrophobic and hydrophilic ends (Figure 1a). Surface tension decreases with increased surfactant concentration on the interface until the bulk solution reaches the critical micelle concentration CMC, and it remains constant thereafter as the excess surfactant in the bulk solution forms micelles (Figure 1b) [*Defay and Prigogine*, 1949; *Miller et al.*, 1994; *Holmberg et al.*, 2003; *Rosen*, 2004; *Israelachvili*, 2011]. The surfactant density on the interface homogenizes rapidly, driven by the surface tension gradient created by heterogeneous concentrations, i.e., Marangoni effect [*Scriven and Sternling*, 1960; *Schramm and Wassmuth*, 1994; *Nikolov et al.*, 2002; *Tadmor*, 2009; *Still et al.*, 2012]. In addition to the adsorption onto gas-liquid "gl" interfaces, surfactants adsorb onto liquid-solid "ls" and gas-solid "gs" interfaces as well; therefore, the effect of surfactants on $\cos\theta$ is not limited to the inverse of T_{gl} [*Chen and Mohanty*, 2013]. Adsorption at interfaces and micelle formation affect the efficiency of surfactants in engineered applications that range from the remediation of NPAL contaminated sites to enhanced oil recovery.

Surfactant adsorption and interfacial concentration are time-dependent and may evolve in response to changes in pore geometry (Figure 1c). The pulmonary surfactant is an example of a bio-engineered system that exploits this effect: surfactant concentration and surface tension vary as alveoli expand and contract facilitating breathing [*Clements et al.*, 1958; *Ghadiali and Gaver*, 2000; *Gerber et al.*, 2006; *Nakahara et al.*, 2010]. The relevance of this geometry-dependent rate effect in porous media such as sediments remains unknown.

This paper reports pressure signatures gathered as fluid interfaces traverse a constriction in a cylindrical capillary tube during advancing and receding tests. The study explores the effect of surfactant concentration, infers transient changes in surfactant concentration at the interface, and identifies pore-scale instabilities.

Table 1. Experimental Study: Fluids[a]

Liquid	Concentration of Surfactant in Water [mg/g]	T_{gl} [mN/m] Commercial Surfactant[b]	T_{gl} [mN/m] SDS[c]	Contact Angle-SDS [°][d] Advancing	Contact Angle-SDS [°][d] Receding
Water	n/a	72		72	51
	0.025		72	73	48
	0.05		71	73	35
Aqueous surfactant solution	0.1	30	70	71	31
	0.25	27	65	70	28
	0.5	26	57	69	28
	1.0	25	46	53	25
	2.5	25	37	28	25
	5.0	26	37	26	25
	10.0	27	37	26	25
	25.0	28	37	25	24
	50.0	29.0			
Alcohol	n/a	24		33	30

[a] The critical micelle concentration of sodium dodecyl sulfate SDS is CMC = 2.4 mg/g at 25°C.

[b] Measured using a ring tensiometer (platinum-iridium ring with a mean circumference of 59.35 mm; the ratio of the ring major radius to the wire radius is 53.2).

[c] From *Prosser and Franses* [2001] and see also *Mysels* [1986].

[d] Measured for water and SDS solutions using images before the necking. Flow rate of 40 μL/h and a front speed of 15 μm/s.

2. Experimental Study

2.1. Fluids: Surface Tension

Four fluids were used in this study: deionized water, alcohol, aqueous surfactant solutions prepared with sodium dodecyl sulfate SDS ($NaC_{12}H_{25}SO_4$—no salt), and solutions prepared with a commercially available surfactant (from safety data sheet, it consists of sodium dodecyl sulfate and sodium laureth sulfate as the main anionic surfactants, less than 5% of ethanol as a cosurfactant, 3–7% of amine oxide as a cationic/zwitterionic surfactant and foam stabilizer, and some sodium chloride). SDS solutions reach the critical micelle concentration at CMC $\approx$ 2.4 mg/g, in agreement with surface tension values in Table 1. The surface tension measured at all concentrations for the commercial surfactant solutions was near the minimum value $T_{gl} = 25.5$ mN/m, thus tested concentrations 0.1–50 mg/g are above the critical micelle concentration (Table 1).

2.2. Pore-Scale Tests: Experimental Procedure

Pore-scale tests were conducted using 75 mm long borosilicate capillary tubes with internal diameter ID = 0.97 mm. A constriction was formed by localized heating and rotation to reach a minimum diameter at the pore throat (constriction length ~3 mm; ID = 0.26 mm for commercial surfactant, and ID = 0.33 mm for tests with SDS solutions, Figure 2). The nominal pore throat size ID $\approx$ 0.3 mm reflects the trade-off between detailed visualization and pressure signature amplitude, and it is an upper bound for fluid flow passages in sandy sediments and sandstones [*Fredrickson et al.*, 1997; *Bloomfield et al.*, 2001; *Bennion and Bachu*, 2006;

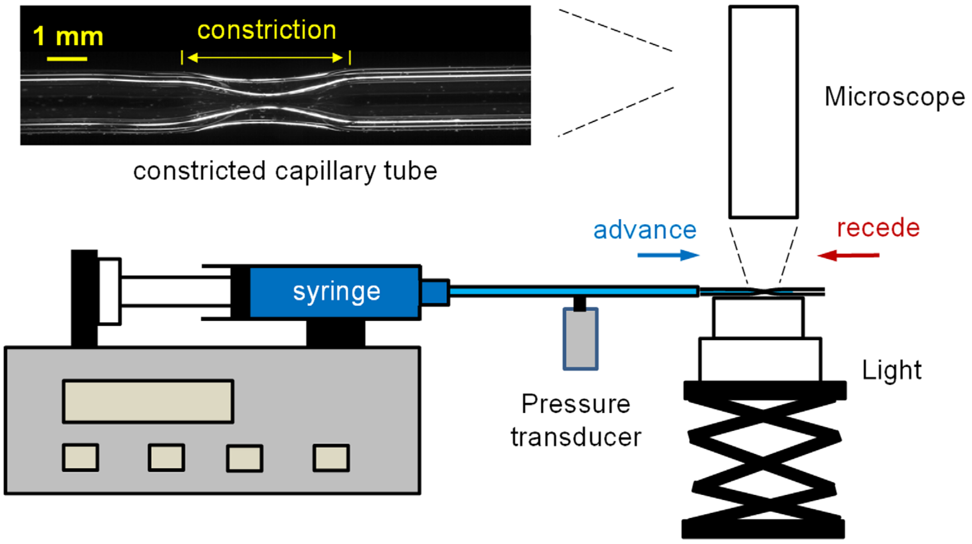

Figure 2. Experimental configuration used to study capillary effects in a constricted capillary tube (microphotograph shown in the inset). Injection flow rates vary from q = 20 to 160 μL/h. See flow conditions in Table 2.

Minagawa et al., 2008]. In the dimensionless space of governing parameters, conditions tested in this study apply to those described in Table 2, which are within the range of many real field situations from NAPL remediation to resource recovery.

Table 2. Experimental Study: Flow Rate and Dimensionless Ratios Re and Ca Calculated for Water[a]

Flow Rate [μL/h]	Velocity [μm/s]	Reynolds Number, Re[b]	Capillary Number, Ca[c]
20	7.5	8×10^{-3}	0.94×10^{-7}
40	15	16×10^{-3}	1.88×10^{-7}
80	30	32×10^{-3}	3.76×10^{-7}
160	60	64×10^{-3}	7.52×10^{-7}

[a] Parameters: fluid velocity v [m/s], pore radius $r = 0.485$ mm, fluid density $\rho = 1000$ kg/m^3, fluid viscosity $\mu = 0.9 \times 10^{-3}$ Pa s, liquid-gas surface tension $T_{lg} = 0.072$ N/m.

[b] The Reynolds number Re compares inertial and viscous forces $Re = 2\rho v r/\mu$.

[c] The capillary number Ca compares viscous and capillary forces $Ca = \mu v/T_{lg}$.

The constricted capillary tube was connected to a microcontrol 5 mL syringe through a stainless steel tube. A pressure transducer mounted next to the inlet was used to monitor the liquid pressure. The general test configuration is sketched in Figure 2.

The syringe pump maintained the preselected flow rate constant during both advancing and receding tests. Imposed flow rates are summarized in Table 2. Propagation velocities and the values of Reynolds number Re and capillary number Ca for water are included in the table; flow conditions remain in the same Reynolds and capillary number Re-Ca regime for all tests conducted in this study (see Re and Ca values in Table 2). Tests were conducted with deionized water first, then alcohol, and finally with surfactant solutions run from the lowest to the highest concentration. Each test consisted of multiple receding-advancing cycles at incrementally higher flow rates.

2.3. Results

Pressure-time (P-t) signatures and concurrent images are recorded for all fluids and injection rates as the liquid-gas interface traverses the tube constriction. A signature recorded during a receding test and selected snapshots are presented in Figure 3. Notice the change in capillary pressure across the pore throat, the

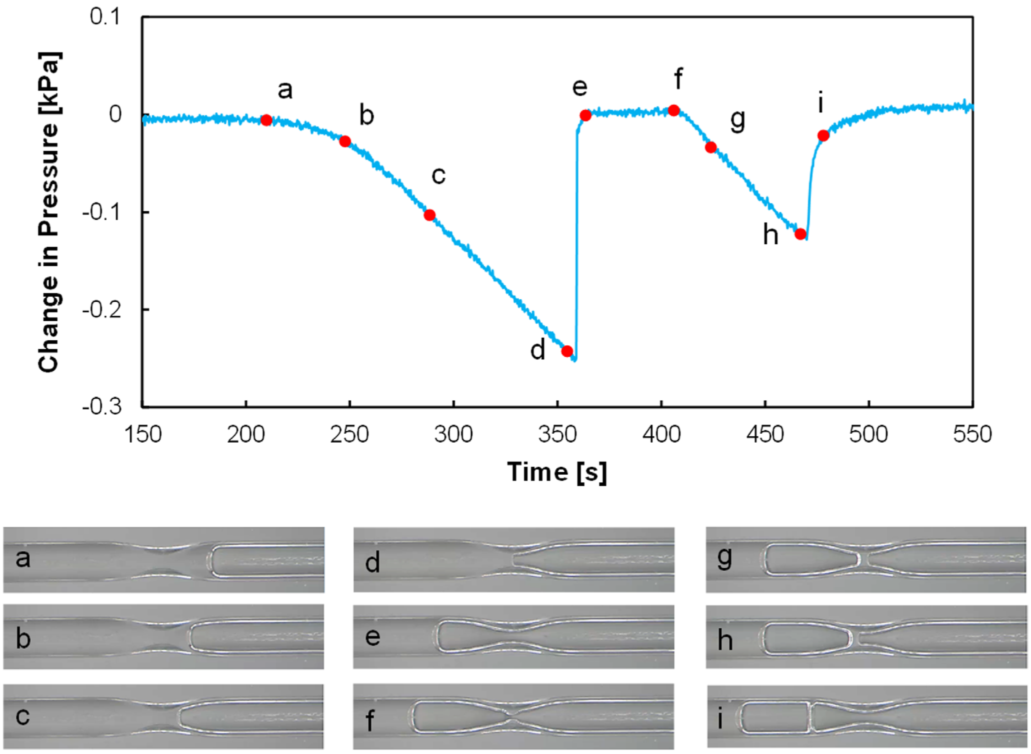

Figure 3. Characteristic pressure signature P-t and selected snapshots—case: SDS 25 mg/g solution during receding test at a flow rate of 20 µL/h. Notice the formation of a liquid plug at the pore constriction leading to the generation of a second pressure pulse.

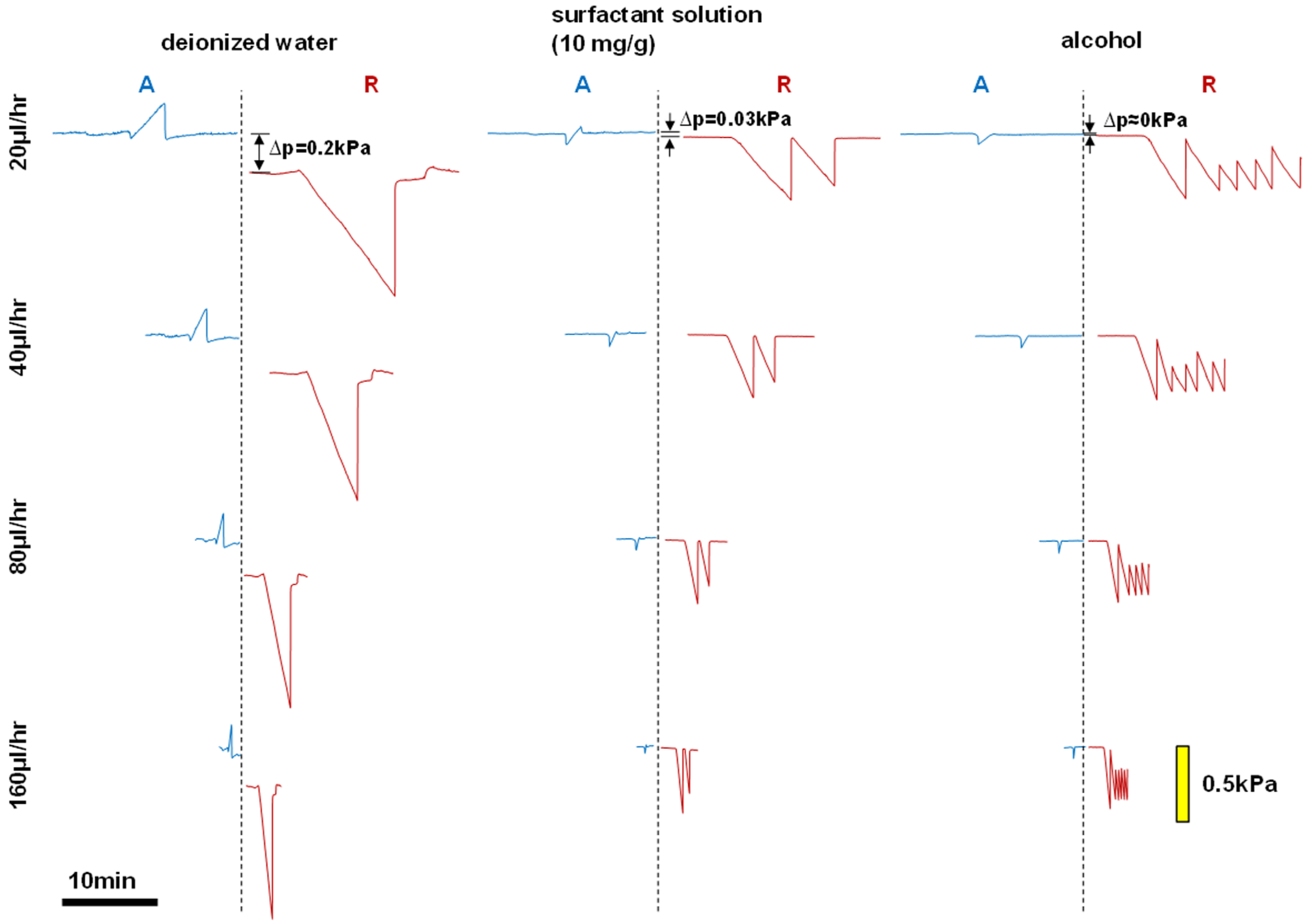

Figure 4. Pressure-time (P-t) signatures recorded as the liquid-gas interface traverses the pore constriction. These pressure-time signatures were obtained with deionized water, commercial surfactant solution, and alcohol during advancing A and receding R tests. Signatures are shown for four different flow rates. For reference, a 10 min scale is shown on the figure.

sudden jump at point-e, the formation of a plug at the pore throat (point-f), and the associated increase in capillary pressure until a new jump takes place at point-h.

Figure 4 shows other P-t signatures in detail. There are marked differences among signatures. Receding tests mobilize significantly higher capillary pressure maxima than advancing tests. During advancing tests, the pressure decreases as the interface moves toward the necking, increases thereafter, and the liquid must be pushed until it suddenly advances past the throat and the pressure drops at once. During receding tests, the water pressure decreases as the interface is retracted toward the necking, reaches a minimum, and suddenly recovers to the steady state value (see Figure 3 for details). The pressure signatures for the 10 mg/g concentration of the commercial surfactant are similar to those for alcohol; both liquids experience repetitive snap-offs and the formation of plugs that block air invasion at the necking. These liquid plugs regenerate very fast, producing oscillatory pressure cycles with a frequency that is proportional to the imposed flow rate, this means that plug formation is faster than the pressure buildup (for the range of flow rates tested in this study).

Figure 5 shows signatures measured at all flow rates for deionized water, solutions prepared with the commercial surfactant and alcohol. To facilitate the comparison, time is normalized t* by the flow rate to highlight similarities among signatures. This complete set of P-t* signatures shows systematic changes with surfactant concentration, but no significant effects of flow rate (within the tested range). The peak pressure decreases as the surfactant concentration increases in all cases. Snap-offs and the formation of repetitive liquid plugs are observed at all flow rates in alcohol and when the concentration of the commercial surfactant exceeds 10 mg/g.

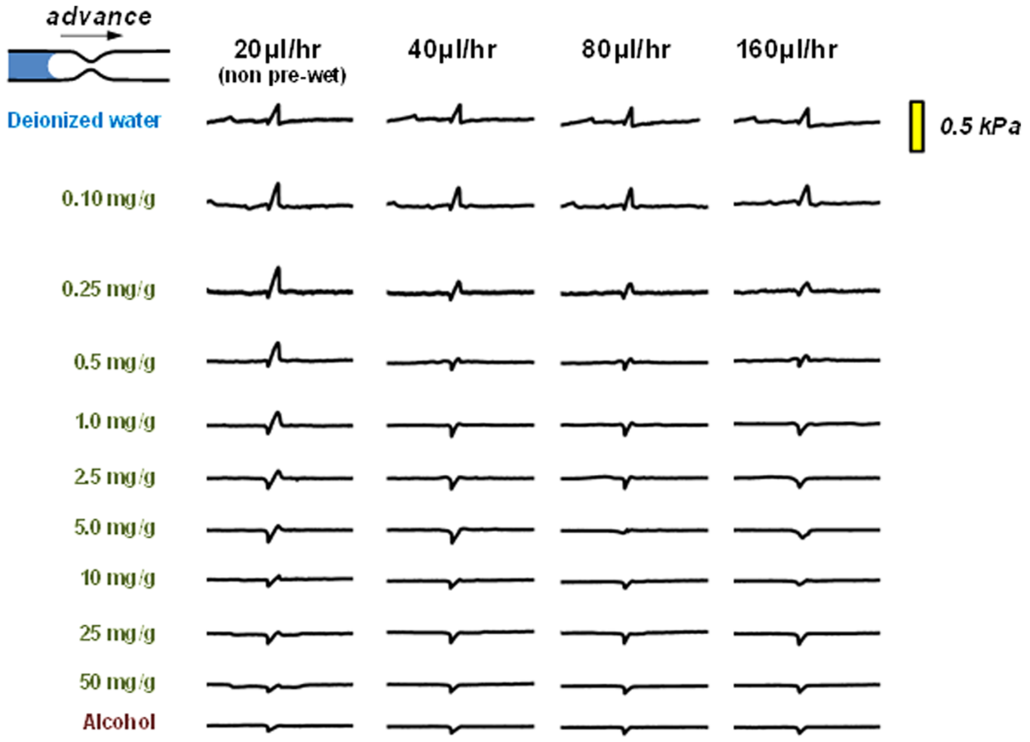

(a) Advancing tests

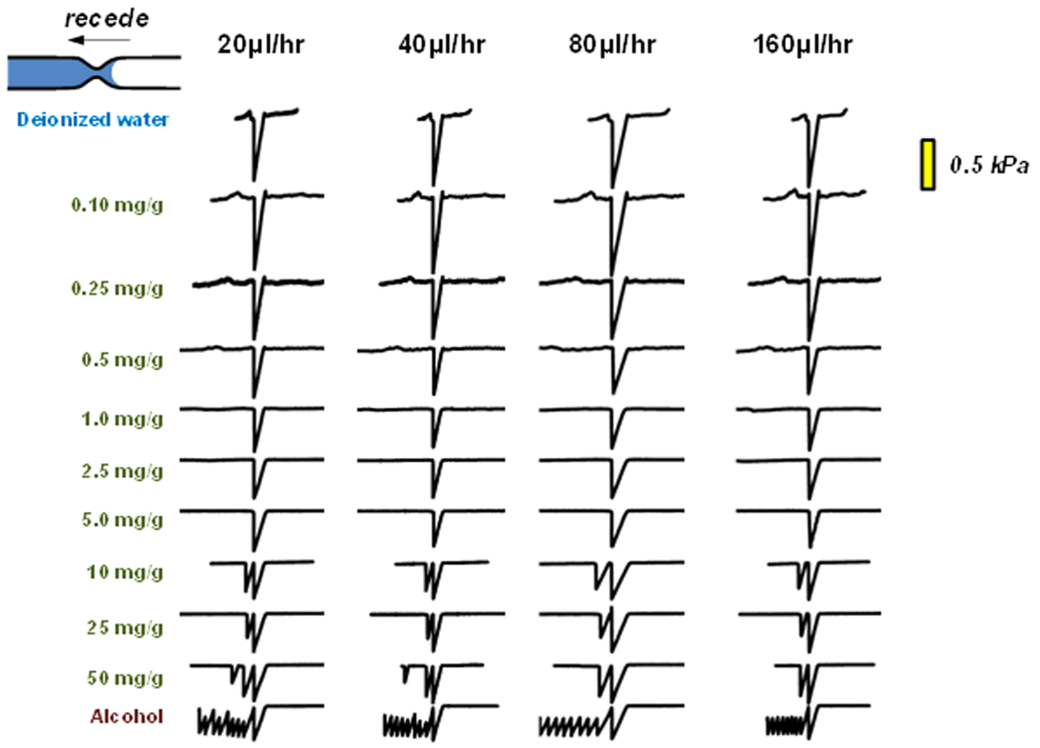

(b) Receding tests

Figure 5. Pressure-time signatures for different fluids across the pore constriction. Time is normalized by the flow rate to highlight similarities among signatures. Cases: (a) advancing and (b) receding tests. Fluids: deionized water, commercial surfactant solutions, and alcohol.

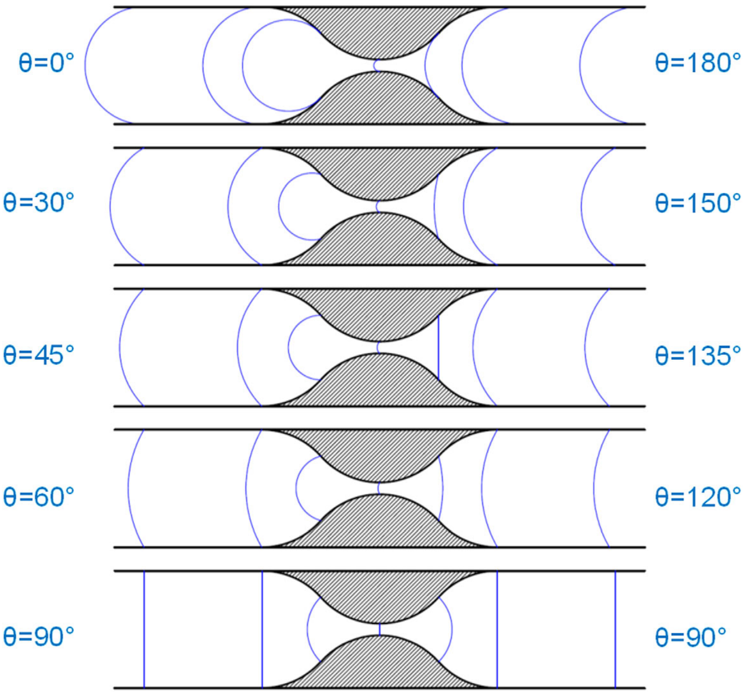

Figure 6. Constant curvature interfaces along a capillary tube with a pore constriction.

3. Analyses and Discussion

3.1. Contact Angle in Capillary Tubes

All test results reported here and complementary static-dynamic tests indicate that the contact angle in advancing θ_{ad} and receding tests θ_{rec} bound the static contact angle θ_{st}, in other words $\theta_{ad} > \theta_{st} > \theta_{rec}$. Advancing and receding contact angles measured in the capillary tube away from the necking are summarized in Table 1; contact angles are similar $\theta_{ad} \sim \theta_{rec}$ when the surfactant concentration approaches and exceeds the critical micelle concentration CMC.

3.2. Capillary Pressure in Noncylindrical Pores

The geometry of the pore affects the generation of capillary pressure [*Purcell*, 1950; *Mason and Morrow*, 1991; *Urso et al.*, 1999]. Let us adopt a pore geometry defined by a double cosine function inspired in the experimentally tested tubes (photograph in Figure 2). Constant curvature interfaces along this pore constriction are sketched for various contact angles in Figure 6. Notice the concave-to-convex transitions for intermediate contact angles.

The local angle α_x between the tube surface at position-x and the flow direction is introduced into the equilibrium equation (refer to Figure 1d) to obtain the modified Laplace equation for the capillary pressure at position-x

$$P_{c,x} = \frac{2T_{gl}\cos\left(\theta - \alpha_x\right)}{r_x}. \tag{1}$$

This equation predicts that the air-liquid interface changes from concave to convex when the argument $(\theta\text{-}\alpha_x) > 90$. The capillary pressure versus position P-x signatures computed using equation 1 are plotted in Figure 7 for the same geometry analyzed in Figure 6. When fluids are perfectly wetting $\theta = 0$, signatures remain alike and the capillary pressure scales linearly with surface tension (Figure 7a). In contrast, there are marked changes in P-x signatures with contact angle, as shown in Figure 7b for the case of an air-water system ($T_{gl} = 72$ mN/m): the capillary pressure changes from negative-to-positive across the pore throat when the contact angle $\theta \rightarrow 90°$. The position of capillary pressure maxima depends on the pore geometry α_x and contact angle θ: the maximum capillary pressure develops at the pore throat when $\theta = 0°$ only. Notice that capillary resistance can develop at a pore constriction even when fluids are considered "wetting."

3.3. Theoretical Versus Experimental Signatures: Instabilities

Trends in measured pressure-time (P-t) signatures exhibit patterns similar to the analytical P-x signatures when the contact angle $\theta \rightarrow 90°$ during advancing tests and is $\theta \rightarrow 0°$ during receding tests (Figures 5 and 7). Such a marked change in contact angle is in agreement with the much larger capillary maxima observed in receding tests compared to advancing tests (all fluids and flow rates—measured values in Table 1).

In contrast to analytical signals, measured signatures reveal sudden pressure changes that last less than the 250 ms sampling interval (Figures 4 and 5—note the transit time across the pore constriction lasts up to 20 min). Sudden changes in advancing and receding tests include (Figure 8):

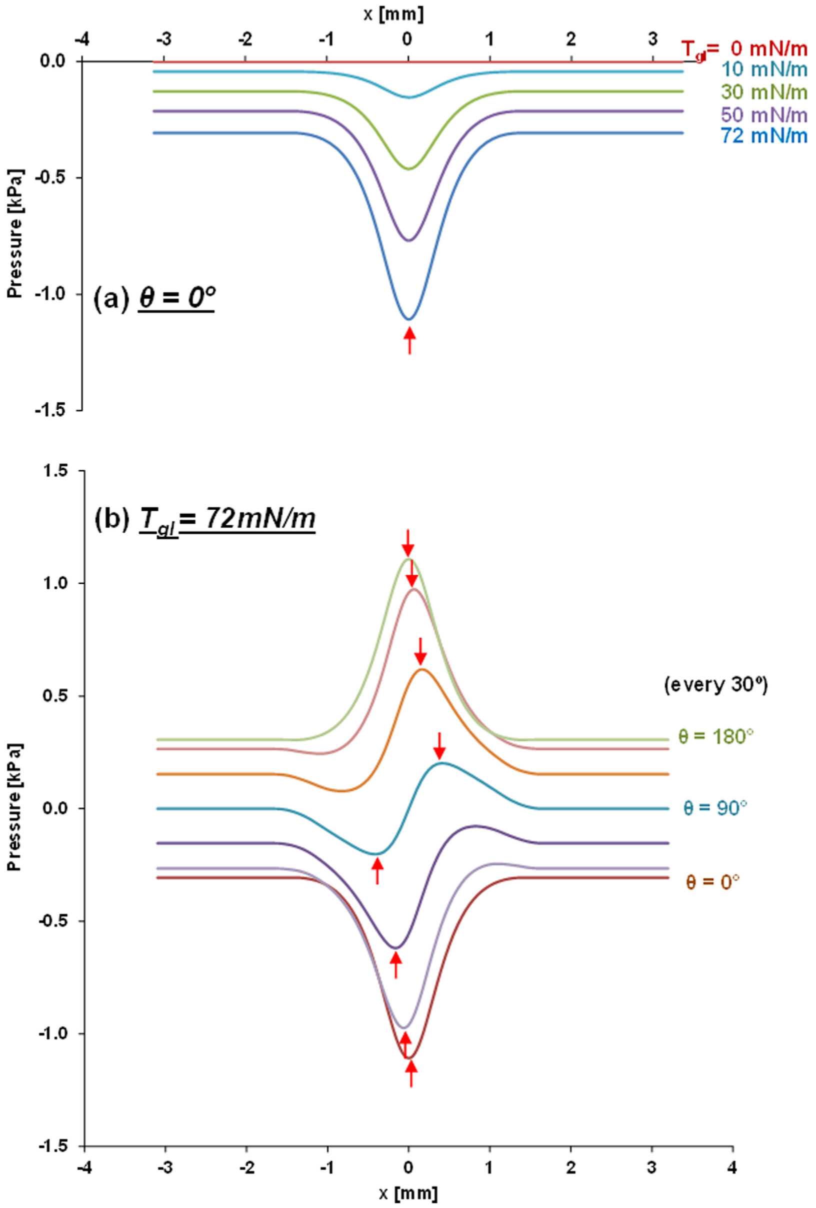

Figure 7. Analytically computed liquid pressure-versus-position P-x signatures as a function of (a) surface tension T_{lg} and (b) contact angle θ. The assumed constriction geometry is a double cosine function. Capillary pressure maxima (shown with red arrows) take place at the pore throat when $\theta = 0°$ only.

- *Advancing tests*. Acceleration before the pore throat. The wetting interface accelerates toward the pore throat driven by increasing capillarity in the narrowing pore ($\theta \rightarrow 90°$, i.e., positive feedback with the pore geometry). The maximum capillary pressure mobilized at the pore throat depends on the system stiffness.
- *Advancing tests*. Jumps after the pore throat. The advancing fluid $\theta \rightarrow 90°$ must be pushed against the capillary resistance until the peak is reached, and then the front accelerates ahead. This "stick-slip" response appears as positive peaks in experimental P-t signatures (Figure 5a) and corresponds to positive humps in analytical P-x signals (Figure 7b).
- *Receding tests*. Jumps at the pore throat. The contact angle tends to $\theta \rightarrow 0°$ and the peak suction is reached at the pore throat; once again, a "stick-slip" instability follows as the resistance decreases beyond the pore throat.

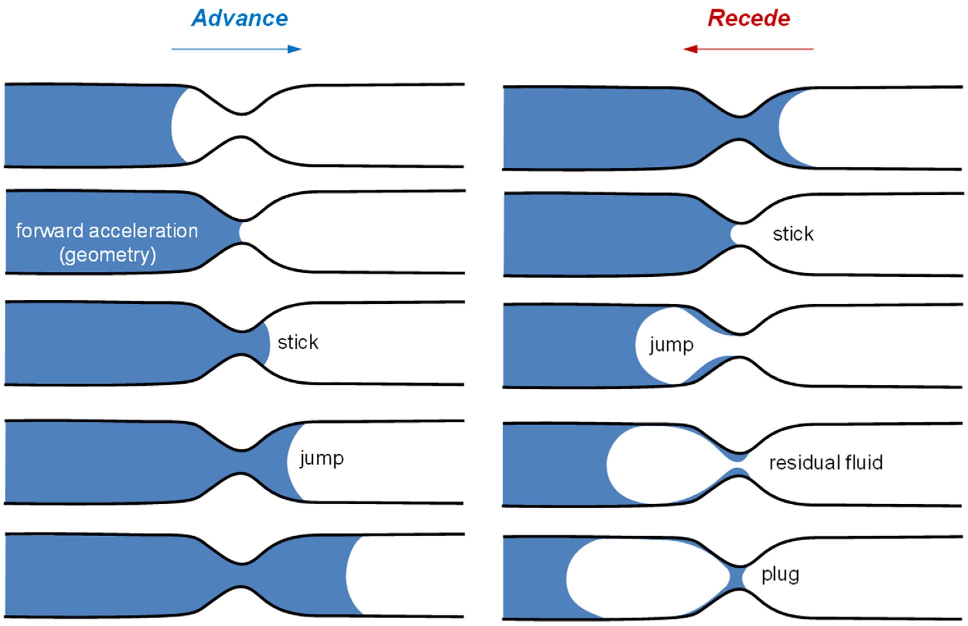

Figure 8. Capillary instabilities during the advancing and receding of wetting fronts across a pore constriction. Liquid plugs often reform during receding tests.

Jumps in advancing and receding tests are analogous to stick-slip behavior in post-peak-softening frictional systems when a soft spring pulls the mass. Similarly, the acceleration toward the pore throat observed in advancing tests is also possible when the capillary-driven fluid mass is restrained by a "soft spring." We conclude that accelerations and jumps take place in all porous media filled with mixed fluids because interfaces can readily adjust at the multiple pore throats that confine a globule; in other words, a jump or acceleration near a pore throat takes place at the expense of fluctuations at all other interfaces.

Stiffness-dependent capillary pressure generation during accelerating wetting fronts and jumps lead to P-t signatures that deviate considerably from theoretically predicted signals. However, measured pressure P values that are unaffected by these instabilities plot over the analytical pressure-position P-x signatures (Figure 9, middle row) when the corresponding x-position for each data point is obtained from the concurrent video recording.

3.4. The Effect of Surfactants on Capillary Pressure Across Pore Throats

Let us select pressures P_a and P_b shown for advancing and receding tests in Figure 10 to avoid instability-controlled biases on measured pressures. The pressure difference $\delta P = P_a - P_b$ is the change in capillary pressure to cross the pore throat. Figure 10 summarizes δP data in advancing and receding tests for all flow rates. These data correspond to tests run with the SDS solutions; similar trends were obtained with the commercial surfactant. The continuous lines are computed using the constriction geometry, together with contact angle and surface tension values listed in Table 1.

The marked differences in capillary pressure δP between values in the upper and lower plots are primarily due to differences in contact angle during advancing ($\theta \rightarrow 90°$: maximum capillary resistance past the pore throat) and receding ($\theta \rightarrow 0°$: maximum suction at the pore throat).

On the other hand, the magnitude of $\delta P = P_a - P_b$ varies with surfactant concentration in both advancing (top) and receding wetting fronts (bottom). In both cases, the measured capillary pressures across the constriction δP are lower than the analytically computed values for solutions with surfactant concentrations in the range of ~0.01–2.4 mg/g, where the upper bound is the critical micelle concentration CMC (Figure 10). We anticipate transient surfactant accumulation at the interface, similar to the mechanism captured in Figure 1c. Differences above the CMC during receding tests may be associated to dynamic stiffening of the receding interface in the presence of surfactants [*Ghadiali and Gaver*, 2000, 2008].

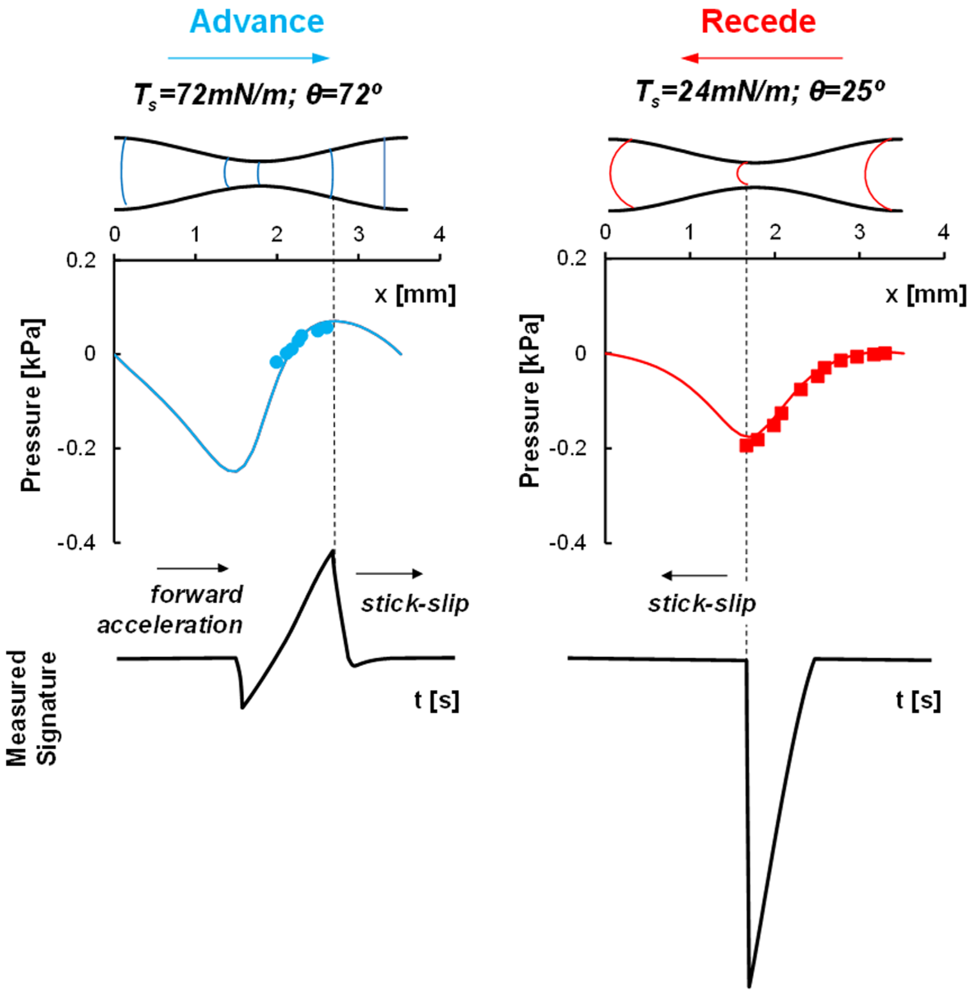

Figure 9. Predicted versus measured pressure signatures during advancing and receding wetting fronts across a pore constriction. Middle row: theoretical pressure-position P-x signatures; the x-position of data points shown on these plots is obtained from the concurrent video recordings. Lower row: measured pressure-time P-t signatures. Note: P-x and P-t signatures are aligned at the stick-slip instability. Left: advancing water (80 μL/h). Right: receding alcohol (80 μL/h).

Overall, data in Figure 10 hint to delayed molecular responses and dynamic interactions that alter surfactant packing at the interface, adsorption-desorption, and nonequilibrium critical micelle CMC concentration [*Huang et al*., 1989; *Schulz and Warr*, 2002; *Zhang and Somasundaran*, 2006; *Ghumare*, 2012].

3.5. Recurrent Plug Formation

Snap-offs and subsequent plug formation has been reported as choke-off instabilities [*Mohanty et al*., 1987], analyzed in relation to film flow [*Lowry and Miller*, 1995], and relates to film rapture and residual water left behind (observed by *Hsu and Hilpert* [2016]). Our results show that wetting liquids tend to form plugs at pore constrictions during receding tests immediately after the stick-slip jump (Figure 3): surface tension forces the residual wetting liquid to migrate toward the pore throat where it contracts to form the plug (sketched in Figure 8). Plug formation is preferentially observed in fluids with low surface tension (e.g., solutions with surfactant near the CMC, and alcohol, Figures 4 and 5b). Complementary tests—not shown here—confirm the formation of plugs in water-wet capillaries during the invasion of oil, and the increased tendency to plug reformation in narrower pore constrictions. Successive pressure spikes in Figures 4 and 5 show that these plugs can break and reform multiple times.

Plugs split the nonwetting fluid into isolated globules and add resistance against fluid flow. Consequently, plugs hinder the extraction on nonwetting fluids from the subsurface, for example during remediation efforts or resource recovery.

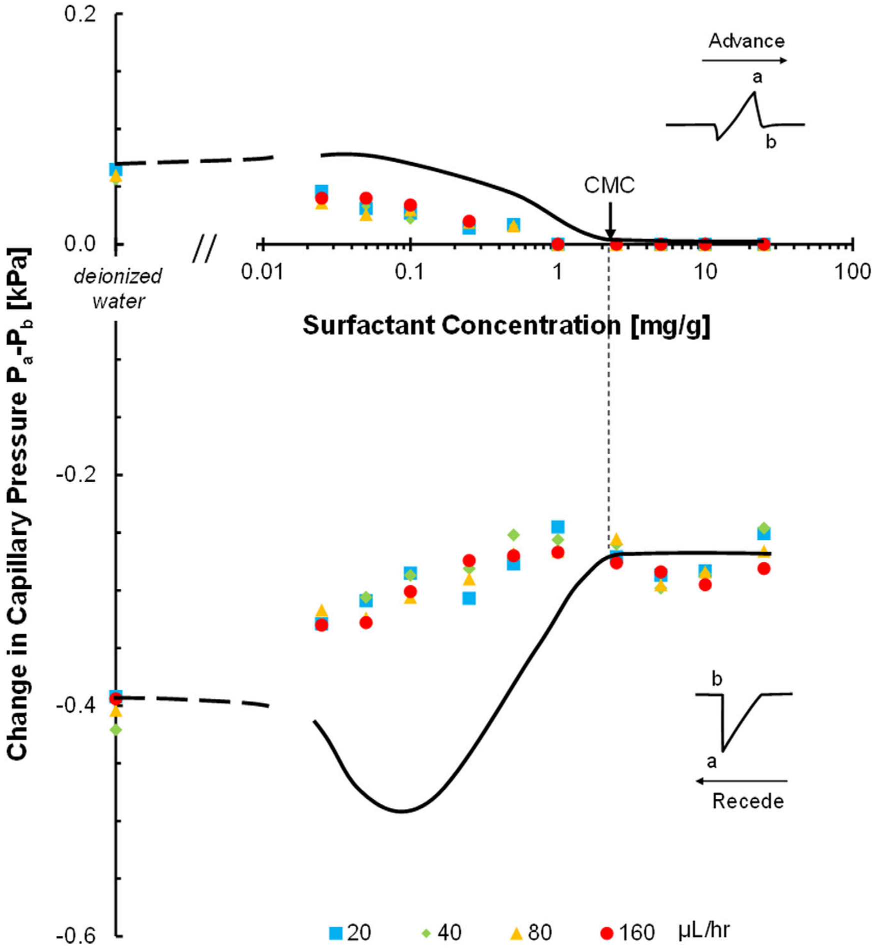

Figure 10. Measured changes in capillary pressure δPc at the pore constriction during advancing and receding tests with SDS solutions. Selected a-and-b pressures avoid biases discussed in the text. Values of δP for deionized water appear on the *Y* axis. The continuous lines are computed using the constriction geometry, the contact angle measured for each solution in the capillary tube before the necking, and surface tension values listed in Table 1.

4. Conclusions

Capillarity controls the distribution and transport of immiscible fluids in soils and fractured rocks; thus, it plays a central role in the evolution of subsurface contamination and remediation, resource recovery, and carbon geological storage.

The measurement of capillary pressure across a pore constriction with concurrent video recording is an information-rich test. The capillary pressure is a function of contact angle, surface tension, and the evolving pore geometry as the fluid interface traverses the pore constriction in advancing and receding tests.

Four distinct instabilities were observed in these experiments: forward acceleration driven by positive feedback from the narrowing pore geometry, stick-slip jump during advancing and receding tests, and snap-offs followed by plug formation in receding wetting fronts. These pore-scale phenomena alter the measured pressure-time signatures.

Contact angle and instabilities are responsible for pronounced differences between pressure signatures recorded during advancing and receding tests, and underlie hysteretic saturation in porous media.

Menisci at pore throats confine fluid globules within porous media. These interfaces can readily adjust; therefore, instabilities at a pore throat take place at the expense of fluctuations at all other bounding interfaces.

For a given transport direction, the amplitude of pressure signatures scales with interfacial tension. However, an interface traversing a pore constriction experiences transient nonequilibrium conditions when aqueous surfactant solutions are involved. The measured capillary pressures cannot be readily anticipated from static-bulk fluid measurements as the transient surface tension can be significantly lower than in static tests. There is some evidence of interface stiffening in high surfactant concentration solutions during receding fronts.

Plugs form when residual annular wetting films/droplets left behind after a jump contract back toward the pore throat. Plug formation is more common when the surface tension is low and pore throats are narrow. Liquid plugs can break and reform multiple times as flow continues. Plugs split the nonwetting fluid into isolated globules and add resistance against fluid flow.

Notation

C	molarity [mol/L].
Ca	capillary number.
CMC	critical micelle concentration [mg/g].
n_a	moles of a surfactant on an adsorbent [mol/g].
P_c	capillary pressure [Pa].
δP	change in capillary pressure across a pore throat [Pa].
q	flow rate [μL/h].
r	pore radius [m].
Re	Reynolds number.
T_{gs}	interfacial tension: gas-solid [N/m].
T_{gl}	interfacial tension: gas-liquid [N/m].
T_{ls}	interfacial tension: liquid-solid [N/m].
V	velocity [m/s].
α	angle between tube surface and mean flow direction [°].
θ	contact angle [°].
μ	viscosity [Pa s].
ρ	density [kg/m^3].

Acknowledgments
Support for this research was provided by the USA Department of Energy and the KAUST endowment. We are grateful to detailed observations and suggestions by the anonymous reviewers. All data sets generated as part of this study are available from the authors.

References

Bechtel, S. E., K. W. Koelling, W. Nguyen, and G. Tan (2002), A new technique for the measurement of the dynamic evolution of surface tension, *J. Colloid Interface Sci.*, *245*(1), 142–162.

Bennion, B., and S. Bachu (2006), The impact of interfacial tension and pore size distribution/capillary pressure character on CO_2 relative permeability at reservoir conditions in CO_2-brine systems, in *SPE/DOE Symposium on Improved Oil Recovery*, Soc. of Pet. Eng., Tulsa, Okla.

Berg, S., et al. (2013), Real-time 3D imaging of Haines jumps in porous media flow, *Proc. Natl. Acad. Sci. U. S. A.*, *110*(10), 3755–3759.

Bico, J., and D. Quere (2002), Rise of liquids and bubbles in angular capillary tubes, *J. Colloid Interface Sci.*, *247*(1), 162–166.

Bloomfield, J. P., D. C. Gooddy, M. I. Bright, and P. J. Williams (2001), Pore-throat size distributions in Permo-Triassic sandstones from the United Kingdom and some implications for contaminant hydrogeology, *Hydrogeol. J.*, *9*(3), 219–230.

Caskey, J. A., and W. B. Barlage (1971), Improved experimental technique for determining dynamic surface tension of water and surfactant solutions, *J. Colloid Interface Sci.*, *35*(1), 46–52.

Cassie, A. B. D., and S. Baxter (1944), Wettability of porous surfaces, *Trans. Faraday Soc.*, *40*, 546–551.

Chatzis, I., and F. A. L. Dullien (1983), Dynamic immiscible displacement mechanisms in pore doublets—Theory versus experiment, *J. Colloid Interface Sci.*, *91*(1), 199–222.

Chen, P. L., and K. K. Mohanty (2013), Surfactant-mediated spontaneous imbibition in carbonate rocks at harsh reservoir conditions, *SPE J*, *18*(1), 124–133.

Clements, J. A., E. S. Brown, and R. P. Johnson (1958), Pulmonary surface tension and the mucus lining of the lungs—Some theoretical considerations, *J. Appl. Physiol.*, *12*(2), 262–268.

Daniel, D. E., L. Alvarez, W. Dershowitz, H. H. Einstein, C. Gable, F. M. Orr, D. Reynolds, J. C. Santamarina, A. M. Shapiro, and K. Singha (2015), *Characterization, Modeling, Monitoring and Remediation of Fractured Rock, Natl.* Academies Press, Washington, D. C.

De Gennes, P. G. (1985), Wetting: Static and dynamics, *Rev. Mod. Phys.*, *57*(3), 827–863.

Defay, R., and I. Prigogine (1949), Surface tension of regular solutions, *Trans. Faraday Soc.*, *46*, 199–204.

Dong, M., and I. Chatzis (1995), The imbibition and flow of a wetting liquid along the corners of a square capillary-tube, *J. Colloid Interface Sci.*, *172*(2), 278–288.

Espinoza, D. N., and J. C. Santamarina (2010), Water-CO_2-mineral systems: Interfacial tension, contact angle, and diffusion-implications to CO_2 geological storage, *Water Resour. Res.*, *46*, W07537, doi:10.1029/2009WR008634.

Essaid, H. I., W. N. Herkelrath, and K. M. Hess (1993), Simulation of fluid distributions observed at a crude-oil spill site incorporating hysteresis, oil entrapment, and spatial variability of hydraulic-properties, *Water Resour. Res.*, *29*(6), 1753–1770.

Essaid, H. I., B. A. Bekins, and I. M. Cozzarelli (2015), Organic contaminant transport and fate in the subsurface: Evolution of knowledge and understanding, *Water Resour. Res.*, *51*, 4861–4902, doi:10.1002/2015WR017121.

Falls, A. H., G. J. Hirasaki, T. W. Patzek, D. A. Gauglitz, D. D. Miller, and T. Ratulowski (1988), Development of a mechanistic foam simulator: The population balance and generation by snap-off, *SPE Reservoir Eng.*, *3*(3), 884–892.

Fredrickson, J. K., et al. (1997), Pore-size constraints on the activity and survival of subsurface bacteria in a late Cretaceous shale-sandstone sequence, northwestern New Mexico, *Geomicrobiol. J.*, *14*(3), 183–202.

Furuberg, L., K. J. Maloy, and J. Feder (1996), Intermittent behavior in slow drainage, *Phys. Rev. E*, *53*(1), 966–977.

Gauglitz, P. A., and C. J. Radke (1989), Dynamics of Haines jumps for compressible bubbles in constricted capillaries, *AIChE J.*, *35*(2), 230–240.

Gens, A. (2010), Soil-environment interactions in geotechnical engineering, *Geotechnique*, *60*(1), 3–74.

Gerber, F., M. P. Krafft, T. F. Vandamme, M. Goldmann, and P. Fontaine (2006), Fluidization of a dipalmitoyl phosphatidylcholine monolayer by fluorocarbon gases: Potential use in lung surfactant therapy, *Biophys. J.*, *90*(9), 3184–3192.

Ghadiali, S. N., and D. P. Gaver (2000), An investigation of pulmonary surfactant physicochemical behavior under airway reopening conditions, *J. Appl. Physiol.*, *88*(2), 493–506.

Ghadiali, S. N., and D. P. Gaver (2008), Biomechanics of liquid-epithelium interactions in pulmonary airways, *Respir. Physiol. Neurobiol.*, *163*(1–3), 232–243.

Ghumare, A. K. (2012), Synthesis, characterization and applications of cationic gemini surfactants, PhD thesis, Inst. of Chem. Technol., Mumbai, India.

Glass, R. J., S. H. Conrad, and W. Peplinski (2000), Gravity-destabilized nonwetting phase invasion in macroheterogeneous porous media: Experimental observations of invasion dynamics and scale analysis, *Water Resour. Res.*, *36*(11), 3121–3137.

Good, R. J. (1966), Estimation of surface energies from contact angles, *Nature*, *212*(5059), 276–277.

Haines, W. B. (1930), Studies in the physical properties of soil: V. The hysteresis effect in capillary properties, and the modes of moisture distribution associated therewith, *J. Agric. Sci.*, *20*, 97–116.

Hirasaki, G. J., C. A. Miller, and M. Puerto (2011), Recent advances in surfactant EOR, *SPE J.*, *16*(4), 889–907.

Hoffman, R. L. (1975), Study of advancing interface: 1. Interface shape in liquid-gas systems, *J. Colloid Interface Sci.*, *50*(2), 228–241.

Holmberg, K., B. Josson, B. Kronberg, and B. Lindman (2003), *Surfactants and Polymers in Aqueous Solution*, John Wiley, Chichester, U. K.

Holtzman, R., M. L. Szulczewski, and R. Juanes (2012), Capillary fracturing in granular media, *Phys. Rev. Lett.*, *108*(26), 264504.

Hsu, S. Y., and M. Hilpert (2016), Pore-scale visualization of the mobilization of a partially wetting droplet, *Adv. Water Resour.*, *95*, 235–245.

Huang, Z., Z. L. Yan, and T. R. Gu (1989), Mixed adsorption of cationic and anionic surfactants from aqueous-solution on silica-gel, *Colloid Surf.*, *36*(3), 353–358.

Iglauer, S., Y. F. Wu, P. Shuler, Y. C. Tang, and W. A. Goddard (2010), New surfactant classes for enhanced oil recovery and their tertiary oil recovery potential, *J. Pet. Sci. Eng.*, *71*(1–2), 23–29.

Israelachvili, J. N. (2011), *Intermolecular and Surface Forces*, Academic, San Diego, Calif.

Johannessen, A. M., and K. Spildo (2013), Enhanced oil recovery (EOR) by combining surfactant with low salinity injection, *Energy Fuel*, *27*(10), 5738–5749.

Kim, S., and J. C. Santamarina (2014), Engineered CO_2 injection: The use of surfactants for enhanced sweep efficiency, *Int. J. Greenhouse Gas Control*, *20*, 324–332.

Kovscek, A. R., and C. J. Radke (1994), Fundamentals of foam transport in porous media, in *Foams: Fundamentals and Applications in the Petroleum Industry*, edited by L. Schramm, pp. 115–163, Am. Chem. Soc., Washington, D. C.

Kovscek, A. R., G. Q. Tang and C. J. Radke (2007), Verification of Roof snap off as a foam-generation mechanism in porous media at steady state, *Colloid Surf. A*, *302*(1–3), 251–260.

Kwok, D. Y., and A. W. Neumann (2000), Contact angle interpretation in terms of solid surface tension, *Colloid Surf. A*, *161*(1), 31–48.

Lenormand, R., C. Zarcone, and A. Sarr (1983), Mechanisms of the displacement of one fluid by another in a network of capillary ducts, *J. Fluid Mech.*, *135*, 337–353.

Lenormand, R., E. Touboul, and C. Zarcone (1988), Numerical-models and experiments on immiscible displacements in porous-media, *J. Fluid Mech.*, *189*, 165–187.

Li, W. Q., R. D. Vigil, I. A. Beresnev, P. Iassonov, and R. Ewing (2005), Vibration-induced mobilization of trapped oil ganglia in porous media: Experimental validation of a capillary-physics mechanism, *J. Colloid Interface Sci.*, *289*(1), 193–199.

Likos, W. J., and N. Lu (2004), Hysteresis of capillary stress in unsaturated granular soil, *J. Eng. Mech.*, *130*(6), 646–655.

Lowry, M. I., and C. T. Miller (1995), Pore-scale modeling of nonwetting-phase residual in porous-media, *Water Resour. Res.*, *31*(3), 455–473.

Lu, N., and W. J. Likos (2004), *Unsaturated Soil Mechanics*, John Wiley, Hoboken, N. J.

Maloy, K. J., A. Hansen, E. L. Hinrichsen, and S. Roux (1992), Experimental measurements of the roughness of brittle cracks, *Phys. Rev. Lett.*, *68*(2), 213–215.

Mason, G., and N. R. Morrow (1991), Capillary behavior of a perfectly wetting liquid in irregular triangular tubes, *J. Colloid Interface Sci.*, *141*(1), 262–274.

Mason, G., and N. R. Morrow (1994), Effect of contact angle on capillary displacement curvatures in pore throats formed by spheres, *J. Colloid Interface Sci.*, *168*(1), 130–141.

Miller, R., P. Joos, and V. B. Fainerman (1994), Dynamic surface and interfacial tensions of surfactant and polymer solutions, *Adv. Colloid Interface*, *49*, 249–302.

Minagawa, H., Y. Nishikawa, I. Ikeda, K. Miyazaki, N. Takahara, Y. Sakamoto, T. Komai, and H. Narita (2008), Characterization of sand sediment by pore size distribution and permeability using proton nuclear magnetic resonance measurement, *J. Geophys. Res.*, *113*, B07210, doi:10.1029/2007JB005403.

Miwa, M., A. Nakajima, A. Fujishima, K. Hashimoto, and T. Watanabe (2000), Effects of the surface roughness on sliding angles of water droplets on superhydrophobic surfaces, *Langmuir*, *16*(13), 5754–5760.

Mohanty, K. K., H. T. Davis, and L. E. Scriven (1987), Physics of oil entrapment in water-wet rock, *SPE Reservoir Eng.*, *2*(1), 113–128.

Morrow, N. R. (1970), Physics and thermodynamics of capillary action in porous media, *Ind. Eng. Chem.*, *62*(6), 32–56.

Mulligan, C. N., R. N. Yong, and B. F. Gibbs (2001), Surfactant-enhanced remediation of contaminated soil: A review, *Eng. Geol.*, *60*(1–4), 371–380.

Mysels, K. J. (1986), Surface tension of solutions of pure sodium dodecyl sulfate, *Langmuir*, *2*(4), 423–428.

Nakahara, H., S. Lee, M. P. Krafft, and O. Shibata (2010), Fluorocarbon-hybrid pulmonary surfactants for replacement therapy—A Langmuir mono layer study, *Langmuir*, *26*(23), 18,256–18,265.

Nikolov, A. D., D. T. Wasan, A. Chengara, K. Koczo, G. A. Policello, and I. Kolossvary (2002), Superspreading driven by Marangoni flow, *Adv. Colloid Interface*, *96*(1–3), 325–338.

Nordbotten, J. M., M. A. Celia, and S. Bachu (2005), Injection and storage of CO_2 in deep saline aquifers: Analytical solution for CO_2 plume evolution during injection, *Transp. Porous Media*, *58*(3), 339–360.

Prosser, A. J., and E. I. Franses (2001), Adsorption and surface tension of ionic surfactants at the air-water interface: Review and evaluation of equilibrium models, *Colloid Surf. A*, *178*(1–3), 1–40.

Pruess, K., and J. Garcia (2002), Multiphase flow dynamics during CO_2 disposal into saline aquifers, *Environ. Geol.*, *42*(2–3), 282–295.

Purcell, W. R. (1950), Interpretation of capillary pressure data, *Pet. Trans. AIME*, *2*(8), 369–371.

Ransohoff, T. C., P. A. Gauglitz, and C. J. Radke (1987), Snap-off of gas-bubbles in smoothly constricted noncircular capillaries, *AIChE J.*, *33*(5), 753–765.

Ransohoff, T. C., and C. J. Radke (1988a), Laminar flow of a wetting liquid along the corners of a predominantly gas-occupied noncircular pore, *J. Colloid Interface Sci.*, *121*(2), 392–401.

Ransohoff, T. C., and C. J. Radke (1988b), Mechanisms of foam generation in glass-bead packs, *SPE Reservoir Eng.*, *3*(2), 573–585.

Reddy, K. R., and R. E. Saichek (2003), Effect of soil type on electrokinetic removal of phenanthrene using surfactants and cosolvents, *J. Environ. Eng.*, *129*(4), 336–346.

Roof, J. G. (1970), Snap-off of oil droplets in water-wet pores, *Soc. Pet. Eng. J.*, *10*(1), 85–90.

Rose, W., and R. W. Heins (1962), Moving interfaces and contact angle rate-dependency, *J. Colloid Sci.*, *17*(1), 39–48.

Rosen, M. J. (2004), *Surfactants and Interfacial Phenomena*, John Wiley, Hoboken, N. J.

Rossen, W. R. (2003), A critical review of Roof snap-off as a mechanism of steady-state foam generation in homogeneous porous media, *Colloid Surf. A*, *225*(1–3), 1–24.

Saenton, S., T. H. Illangasekare, K. Soga, and T. A. Saba (2002), Effects of source zone heterogeneity on surfactant-enhanced NAPL dissolution and resulting remediation end-points, *J. Contam. Hydrol.*, *59*(1–2), 27–44.

Sandnes, B., E. G. Flekkoy, H. A. Knudsen, K. J. Maloy, and H. See (2011), Patterns and flow in frictional fluid dynamics, *Nat. Commun.*, *2*, 288.

Schramm, L. L., and F. Wassmuth (1994), Foams: Basic principles, in *Foams: Fundamentals and Applications in the Petroleum Industry*, edited by L. Schramm, Am. Chem. Soc., Washington, D. C.

Schulz, J. C., and G. G. Warr (2002), Adsorbed layer structure of cationic and anionic surfactants on mineral oxide surfaces, *Langmuir*, *18*(8), 3191–3197.

Scriven, L. E., and C. V. Sternling (1960), Marangoni effects, *Nature*, *187*(4733), 186–188.

Sharma, R., and D. S. Ross (1991), Kinetics of liquid penetration into periodically constricted capillaries, *J. Chem. Soc. Faraday Trans.*, *87*(4), 619–624.

Shin, H., and J. C. Santamarina (2010), Fluid-driven fractures in uncemented sediments: Underlying particle-level processes, *Earth Planet Sci. Lett.*, *299*(1–2), 180–189.

Siebold, A., M. Nardin, J. Schultz, A. Walliser, and M. Oppliger (2000), Effect of dynamic contact angle on capillary rise phenomena, *Colloid Surf. A*, *161*(1), 81–87.

Song, W., and A. R. Kovscek (2015), Functionalization of micromodels with kaolinite for investigation of low salinity oil-recovery processes, *Lab Chip*, *15*(16), 3314–3325.

Still, T., P. J. Yunker, and A. G. Yodh (2012), Surfactant-induced Marangoni eddies alter the coffee-rings of evaporating colloidal drops, *Langmuir*, *28*(11), 4984–4988.

Stokes, J. P., D. A. Weitz, J. P. Gollub, A. Dougherty, M. O. Robbins, P. M. Chaikin, and H. M. Lindsay (1986), Interfacial stability of immiscible displacement in a porous-medium, *Phys. Rev. Lett.*, *57*(14), 1718–1721.

Tadmor, R. (2009), Marangoni flow revisited, *J. Colloid Interface Sci.*, *332*(2), 451–454.

Thomson, W. (1886), Capillary attraction, *Nature*, *34*, 270–272.

Trojer, M., M. L. Szulczewski, and R. Juanes (2015), Stabilizing fluid-fluid displacements in porous media through wettability alteration, *Phys. Rev. Appl.*, *3*(5), 054008.

Urso, M. E. D., C. J. Lawrence, and M. J. Adams (1999), Pendular, funicular, and capillary bridges: Results for two dimensions, *J. Colloid Interface Sci.*, *220*(1), 42–56.

Valvatne, P. H., and M. J. Blunt (2004), Predictive pore-scale modeling of two-phase flow in mixed wet media, *Water Resour. Res.*, *40*, W07406, doi:10.1029/2003WR002627.

Vargaftik, N. B., B. N. Volkov, and L. D. Voljak (1983), International tables of the surface tension of water, *J. Phys. Chem. Ref. Data*, *12*(3), 817–820.

Washburn, E. W. (1921), The dynamics of capillary flow, *Phys. Rev.*, *17*, 273–283.

Weislogel, M. M., and S. Lichter (1998), Capillary flow in an interior corner, *J. Fluid Mech.*, *373*, 349–378.

Wenzel, R. N. (1936), Resistance of solid surfaces to wetting by water, *Ind. Eng. Chem.*, *28*(8), 988–994.

Xue, H. T., Z. N. Fang, Y. Yang, J. P. Huang, and L. W. Zhou (2006), Contact angle determined by spontaneous dynamic capillary, *Chem. Phys. Lett.*, *432*(1–3), 326–330.

Young, T. (1804), An essay on the cohesion of fluids, *Philos. Trans. R. Soc. London*, *95*, 65–87.

Zhang, R., and P. Somasundaran (2006), Advances in adsorption of surfactants and their mixtures at solid/solution interfaces, *Adv. Colloid Interface*, *123*, 213–229.

Zhao, B. Z., C. W. MacMinn, and R. Juanes (2016), Wettability control on multiphase flow in patterned microfluidics, *Proc. Natl. Acad. Sci. U. S. A.*, *113*(37), 10,251–10,256.